IOPscience iopscience.iop.org

Home Search Collections Journals About Contact us My IOPscience

Implementation of integrated 1D hybrid phononic crystal through miniaturized programmable virtual inductances

This content has been downloaded from IOPscience. Please scroll down to see the full text.

2017 Smart Mater. Struct. 26 067001

(http://iopscience.iop.org/0964-1726/26/6/067001)

View the table of contents for this issue, or go to the journal homepage for more

Download details:

IP Address: 152.96.212.170
This content was downloaded on 11/05/2017 at 08:22

Please note that terms and conditions apply.

You may also be interested in:

Multi-resonant piezoelectric shunting induced by digital controllers for subwavelength elastic wave attenuation in smart metamaterial
Gang Wang, Jianqing Cheng, Jingwei Chen et al.

Electron–phonon metamaterial featuring nonlinear tri-interleaved piezoelectric topologies and its application in low-frequency vibration control
Bin Bao, Daniel Guyomar and Mickaël Lallart

Attenuation of transverse waves by using a metamaterial beam with lateral local resonators
Hsin-Haou Huang, Chi-Kuang Lin and Kwek-Tze Tan

Vibration and wave propagation attenuation for metamaterials by periodic piezoelectric arrays with high-order resonant circuit shunts
Wanlu Zhou, You Wu and Lei Zuo

Multimodal vibration damping of a beam with a periodic array of piezoelectric patches connected to a passive electrical network
B Lossouarn, J F Deü and M Aucejo

Manipulating waves by distilling frequencies: a tunable shunt-enabled rainbow trap
Davide Cardella, Paolo Celli and Stefano Gonella

Design and analysis of vibration energy harvesters based on peak response statistics
S Adhikari, M I Friswell, G Litak et al.

Low-frequency vibration isolation in sandwich plates by piezoelectric shunting arrays
Shengbing Chen, Gang Wang and Yubao Song

IOP Publishing Smart Materials and Structures
Smart Mater. Struct. **26** (2017) 067001 (9pp) https://doi.org/10.1088/1361-665X/aa6cf7

Technical Note

Implementation of integrated 1D hybrid phononic crystal through miniaturized programmable virtual inductances

Edgar A Flores Parra[1], Andrea Bergamini[2], Lars Kamm[3], Paul Zbinden[3] and Paolo Ermanni[1]

[1] ETH Zürich, Composite Materials and Adaptive Structures Laboratory, Leonhardstrasse 21, CH-8092 Zürich Switzerland
[2] Empa, Materials Science and Technology, Laboratory for Mechanical Integrity of Energy Systems, Überlandstrasse 129, CH-8600, Dübendorf, Switzerland
[3] Hochschule für Technik, Institut für Mikroelectronik und Embedded Systems, Oberseestrasse 10, CH-8640, Rapperswil, Switzerland

E-mail: edgarf@ethz.ch

Received 22 February 2017, revised 5 April 2017
Accepted for publication 12 April 2017
Published 2 May 2017

Abstract

This paper reports on the first implementation of an integrated programmable hybrid phononic crystal (hPC) for wave propagation control. At the core of the novel hPC is a newly developed and tested miniaturized array of virtual floating inductances with programmable properties. The inductance is the building block for a discrete programmable electrical transmission line aimed at wave propagation control in a 1D hPC. The hybrid characteristic is the result of the coupling between a mechanical waveguide in the form of an elastic beam, and an electrical transmission line. The medium features attenuation of mechanical wave motion due to an energy transfer to the electrical domain. Over the frequency range of wave attenuation the dispersion curves of the hPC are characterized by eigenvalue mode veering. An analytical model, based on the transfer matrix method is presented, to expeditiously calculate the dispersion curves of the hPC. Furthermore, this paper provides numerical and experimental transmittance results which validate the efficiency and tunability of the programmable electrical transmission line. The novelty of this contribution is an analytical model for calculating the dispersion curves of the 1D hPC, and a miniaturized programmable virtual inductance which gives way to a 'smart' material.

Keywords: piezoelectric, electrical transmission line, programmable, virtual inductance, wave propagation, dispersion

(Some figures may appear in colour only in the online journal)

1. Introduction

Increased interest has emerged in attenuation of mechanical vibrations by controlling elastic waves with periodic arrangements of piezoelectric shunts. Most of the past studies with passive shunts have focused on reduction of structural vibrations with arrays of locally shunted piezoelectric elements [1–3]. To a lesser extent, schemes with interconnected piezoelectric shunts have been also investigated [4–6]. The effect of interconnected piezoelectric elements on the dynamic behavior of a structure, as well as the synthesis of analog circuits, to control multi-modal vibration damping has been explored, namely by dell'Isola *et al* [6–9]. While the different reported configurations of passive shunts achieve their objective of producing frequency regions of high attenuation or reducing the amplitude of specific modes, the

 © 2017 IOP Publishing Ltd Printed in the UK

Table 1. List of components of PFVI.

Quantity	Name	Value	Packaging
5	C_1, C_2, C_3, C_6, C_7	100 nF	0402 SMD
1	C_4	10 nF	0402 SMD
1	C_5	1 nF	0402 SMD
2	C_8, C_9	10 μF/25 V	0603 SMD
1	IC1	AD5290	MSOP-10
3	R_1, R_5, R_6	100 Ω	0402 SMD
3	R_2, R_3, R_4	3.9 kΩ	0402 SMD
1	R_7	360 Ω	0402 SMD
1	X_1	AD8034	SOT-23/8
1	X_2	AD8033	SC70-5
1	X_3	NC7WZ16P6	SC70-6

Table 2. Electrical characteristics of PFVI.

Parameter	Condition	Value
Analog supply voltage		$\pm$12 V
Digital supply voltage		5 V
Analog supply current	MAX	$\pm$15 mA
Digital supply current	MAX	1 mA
Power	MAX	365 mW
Input voltage	MAX	$\pm$10 V
Input current	MAX	$\pm$2 mA
Output voltage		$\pm$10 V
Output current		$\pm$2 mA
Bandwidth	$R_L > 10\,\Omega$	10 kHz
Quality	Forward	>50
	Backward	<50
Tolerance	$L \leqslant 2$ H	$\pm$150 mH
	$L > 2$ H	$\pm$70 mH

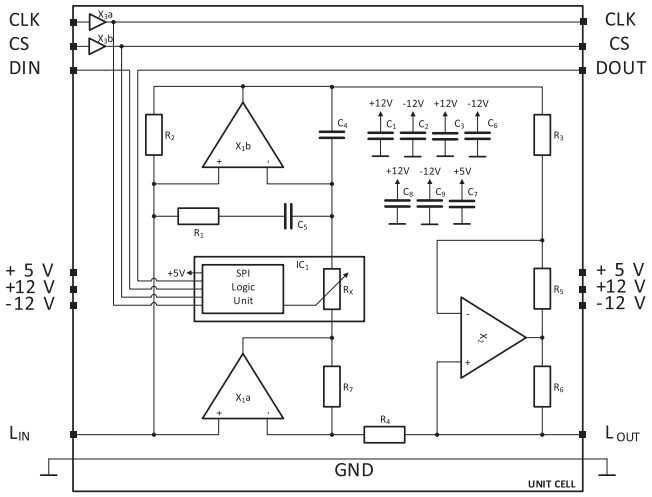

Figure 1. Analog circuit of PFVI.

electrical components which have enabled such shunts have remained relatively rudimentary, i.e.: difficult to tune, too large to integrate as part of the structure [10]. This paper reports on the design, fabrication and testing of an integrated 1D hybrid phononic crystal (hPC) with a unit cell comprised of miniaturized programmable floating virtual inductance (PFVI) for wave propagation control. The hybrid term results from coupling between a mechanical waveguide in the form of an elastic beam, and the electrical transmission line formed from interconnecting multiple PFVI.

Bandgaps in phononic crystals (PCs) emerge from periodic modulations of mass density and/or elastic constants [11, 12] of the material resulting from the basis of the crystal (e.g. diatomic materials [13]). Such band gaps exist for wavelengths on the order of the unit cell size. Conversely, in metamaterials (MM), the inclusion of suitably designed locally resonating units allow for the sub-wavelength modification of the dispersive properties of a medium, as reported by Liu, amongst others, in the mechanical domain [14]. In both PCs and MMs, waves propagate through a mechanical medium and interact with 'inclusions' that either scatter them to generate destructive interference at certain wavenumbers, or that absorb and dissipate energy through local resonances. In many of the reported materials, the nature of the inclusions is purely mechanical [14–16]. In other cases, adaptive materials are exploited to modify the unit cell geometry [17], and tune the properties of the locally resonating units [18–20] or modify the connectivity of a PC [21]. In the latter cases, the electrical domain of the unit cell is self-contained, exchanging energy only with the mechanical domain of the unit cell, thus acting as an inclusion in the mechanical medium. As a result, the mechanical domain of the unit cell is the only pathway for the exchange of energy between cells.

The work of Bergamini *et al* [4] showed that weak coupling interaction between modes of mechanical and electrical waveguides can lead to wave attenuation, as a result of an energy exchange between them. These mode interactions can be classified into veering, crossing and lock-in as discussed by Mace *et al* [22].

Even though, the results of this paper build on an already documented physical phenomenon for the control of elastic waves, this work presents a technological bridge between theory and practical implementation. The interconnected virtual inductances used in the work by Bergamini *et al* [4] proved the physical phenomenon of controlling waves with a 1D hPC. However, the circuits were multiple times larger than the unit cell, and could reliably simulate a limited range of inductance values $0\,\text{H} < L < 1\,\text{H}$. These circuits also had the disadvantage of being impractical for tunning as each one had to be manually adjusted, by setting the resistance value of a conventional potentiometer. The novelty of this contribution is the development of a unit cell size PFVI, capable of achieving inductance values two orders of magnitude greater than real inductances of similar dimensions while ensuring a stable transmission line formed by a daisy chain of PFVI circuits. Moreover, each PFVI on the transmission line is programmable by interfacing with a computer using the GUI shown in figure 2. To the authors' knowledge, this is the first time a programmable transmission line has been implemented to control the propagation of mechanical waves. Lastly, an

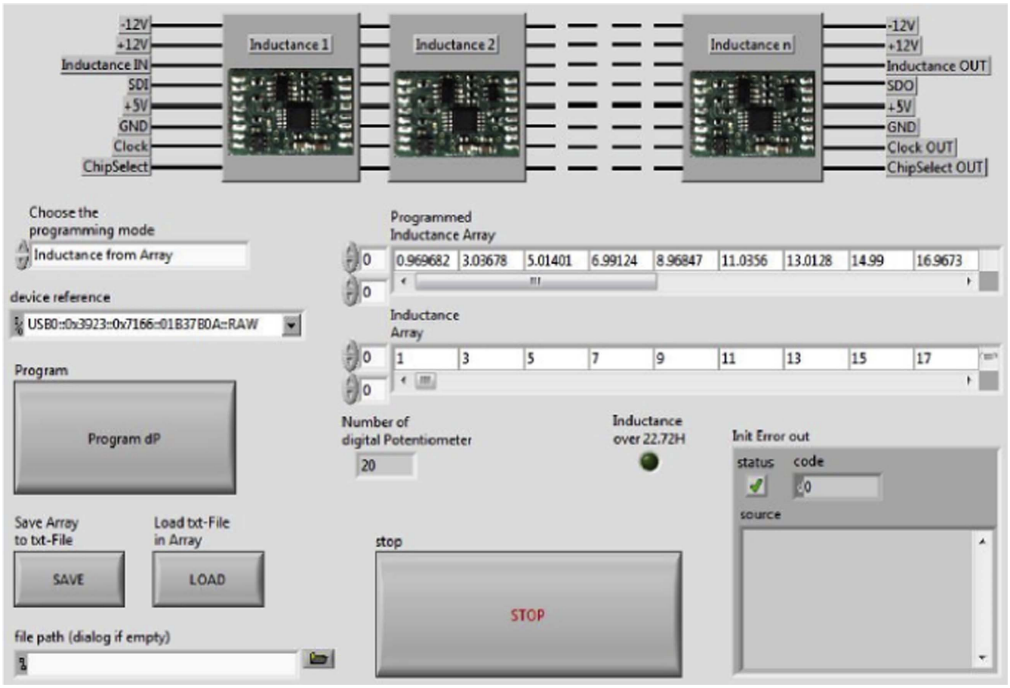

Figure 2. Illustration of interconnected circuits with corresponding input and output connections, as well as LabVIEW graphical user interface (GUI) for programming of the inductances.

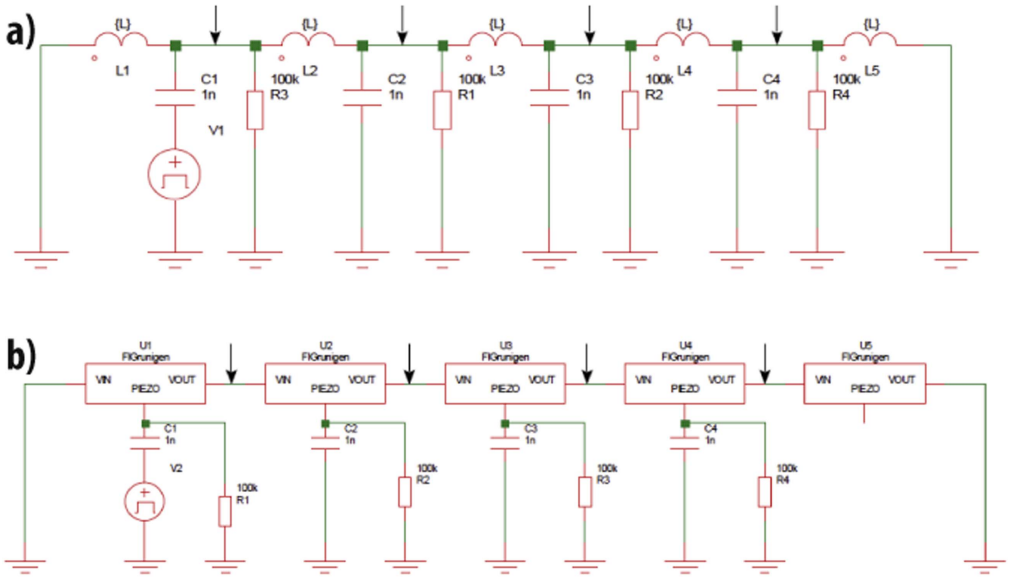

Figure 3. (a) LTSpice model of transmission line with ideal inductances. (b) LTspice model of transmission line with programmable floating virtual inductances.

analytical model to calculate the dispersion curves the 1D hPC is presented. The model is based on the transfer matrix method, and is similar to the one presented by Ruzzene [23]. However, the model presented here accounts for the interconnection between the piezoelectric shunts.

2. Design of PFVI

For the development of the miniaturized PFVI we chose the circuit designed by von Grunigen [24] based on its high quality factor and good stability. The circuit design was implemented in surface mount technology (SMT), to fit a unit cell size 10 by 15 mm that was deemed appropriate based on previous work. The electrical characteristics of the PFVI are given in table 2. The analog circuit of the PFVI is depicted in figure 1, and its component list is given in table 1.

The functionality of the PFVI was first numerically tested in LTSpice, by comparing five interconnected circuits to the equivalent number of ideal inductances, figure 3. The LTSpice simulations of the circuits, and ideal inductances were then validated against experimental measurements as

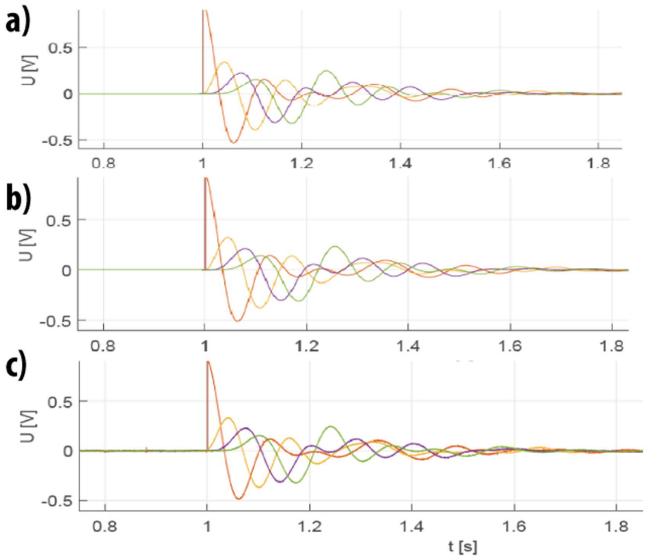

Figure 4. (a) LTspice simulation measurements of a 5 unit cell transmission line with ideal inductances. (b) LTspice simulation measurements of a 5 unit cell transmission line with virtual inductances. (c) Experimental measurements of a 5 unit cell transmission line with virtual inductances.

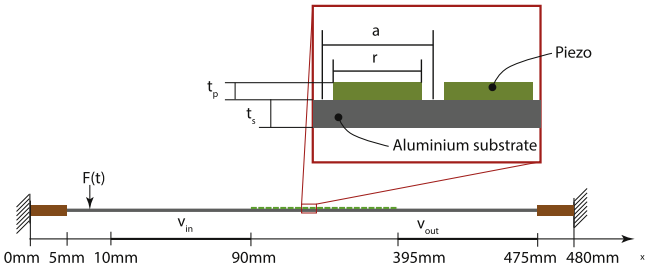

Figure 5. Overview and dimensions of the investigated finite hPC. The dimensions a, t_p, t_s are detailed in the text.

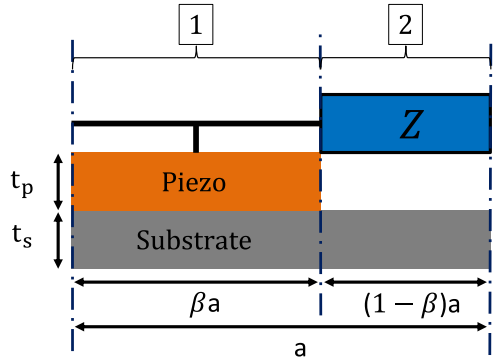

Figure 6. Unit cell illustration showing the aluminum substrate, the piezoelectric element, and electrical impedance separated into two subregions (1 and 2).

seen in figure 4. It is important to note, that unlike a real inductance the behavior of the circuit is not necessarily symmetric since the input and output impedances are different. Hence, waves traveling from left-to-right and from right-to-left may not behave identically.

Since the a virtual inductance is also comprised of active components, it requires a power source to provide the voltages and current given in table 2 for operation. The circuit was powered using an Agilent E3631A 80W triple output power supply.

With the hardware in place, the next step was to implement the programmable capabilities. To this end the line was design to interface with a computer using a National Instruments NI USB-8451 as seen in figure 8. The use of a serial peripheral interface (SPI) allowed for programming of all the circuits connected in a daisy chain. The SPI bus is a synchronous serial communication interface used for communicating over short distances. Using the SPI interface called for four connections linking the computer to the programmable circuits. The interface starts communication by setting the chip select (CS) line logic to zero. The data is clocked through the serial shift registers in the daisy chain configuration. The transfer is complete when all data values are shifted and the CS line logic is set to one. The inductance of all, or each individual PFVI can be set to any value between 1 and 22 H with the resolution given in table 2.

The quality in the production of the transmission line comprised of 21 interconnected PFVI circuits, in particular due to the difficulty of soldering of the SMT components, the fabrication process was ensured by outsourcing to a commercial supplier. The 4 layer PFVI circuits were printed on a 0.9 mm PCB FR4 board.

3. Numerical calculation of the transmittance

For the numerical transmittance and dispersion studies, presented in the following sections, the host structure was made of aluminum with Young's Modulus $E_s = 69$ GPa, density $\rho_s = 2700\,\mathrm{kg\,m^{-3}}$, Poisson's ratio $\nu = 0.33$ and thickness $t_s = 1$ mm. The material of the piezoelectric element was PIC151 with the open circuit Young's Modulus $E_p^D = 77.4$ GPa, density $\rho_p = 7760\,\mathrm{kg\,m^{-3}}$, compliance constant $S_{E_{11}} = 1.5 \times 10^{-11}\,\mathrm{m^2\,N^{-1}}$, permittivity in the polarization direction $\epsilon_{33}^T/\epsilon_0 = 2400$, coupling coefficient $k_{31} = 0.37$.

The numerical transmittance calculation was carried out with COMSOL Multiphysics. As seen in figure 5 we considered an aluminum beam with a thickness $t_s = 1$ mm, width $b = 10$ mm and a total length of $L_T = 480$ mm. In the center portion of the structure, an hPC with unit cell size, $a = 15$ mm, was added, consisting of 20 unit cells positioned between 90 and 395 mm from the origin, each had piezoelectric elements with radius $r = 5$ mm and thicknesses $t_p = 0.5$ mm. The superscript, s, refers to the substrate which serves as the host structure, while the subscript, p, refers to the piezoelectric element. Lastly, the inductive elements were modeled using the electric circuit physics of COMSOL. The inductances values were the same as those used in the calculation of the dispersion curves, in order to establish a direct correlation between the dispersion curves and the transmittance of the hPC. The system was excited mechanically by a discrete force F applied 7.5 mm from the origin, figure 5. The steady state response of the system was calculated over the frequency range of interest.

4. Transfer matrix inverse dispersion

The dispersion curves of the hPC were calculated using the transfer matrix method [23]. The unit cell was divided into the two subregions illustrated in figure 6. The modeling was based on the Euler–Bernoulli beam theory. The first subregion, with length βa, consists of the aluminum substrate and the piezoelectric element. The second subregion, with length $(1-\beta)a$, is characterized by part of the substrate and the electrical impedance. The transfer matrices were computed separately for each subregion. This dispersion model is two-dimensional, thus, for a piezoelectric element with radius $r = 5$ mm, a unit cell of length $a = 15$ mm, and an out-of-plane width, $b = 10$ mm, the coefficient $\beta = 0.52$ was obtained.

4.1. Modeling subregion 1

The system of equations, equations (1)–(6), for the first subregion are obtained from the force and moment equilibria on the infinitesimal element shown in figure 7, where: w is the beam deflection, M_b is the bending moment, Q is the shear force, V is the voltage, I is the current, and ω the angular frequency. Harmonic excitation is assumed to simplify the time derivatives, $\dot{()} = \mathrm{i}\omega()$.

$$\frac{\mathrm{d}w}{\mathrm{d}x} = w_x, \tag{1}$$

$$EI\frac{\mathrm{d}w_x}{\mathrm{d}x} = EIw_{xx} = M_b + \alpha V\left(\frac{t_p}{2} + z_c\right), \tag{2}$$

$$\frac{\mathrm{d}Q}{\mathrm{d}x} = -m\omega^2 w, \tag{3}$$

$$\frac{\mathrm{d}M_b}{\mathrm{d}x} = -Q, \tag{4}$$

$$\frac{\mathrm{d}V}{\mathrm{d}x} = 0, \tag{5}$$

$$\frac{\mathrm{d}I}{\mathrm{d}x} = -\mathrm{i}\omega\alpha w_{xx}\left(\frac{t_p}{2} + z_c\right) - \mathrm{i}\omega C_p' V. \tag{6}$$

Substituting w_{xx}, obtained the bending stiffness equation (2), into equation (6), we obtain equation (7).

$$\frac{\mathrm{d}I}{\mathrm{d}x} = -\mathrm{i}\omega\alpha w_x\left(\frac{t_p}{2} + z_c\right) - \mathrm{i}\omega V\left(C_p' + \frac{\alpha^2}{EI}\left(\frac{t_p}{2} + z_c\right)^2\right). \tag{7}$$

Equations (9) and (12) describe the constants m and Cp', which are the mass and capacitance per unit length. Equation (11), describes the coupling factor α, while the bending stiffness of the bilayer beam is given by equation (8). The bending stiffness was calculated by summing up the contributions of the piezoelectric element, and the substrate, considering their distance from the neutral axis, z_c given by equation (10), and utilizing the parallel axis theorem.

$$\begin{aligned} EI &= E_s I_s + E_p I_p \\ &= b\left(E_s\left(\frac{bt_s^3}{12} + t_s(t_s - z_c)^2\right) + E_p\left(\frac{bt_p^3}{12} + t_p(t_p + z_c)^2\right)\right), \end{aligned} \tag{8}$$

$$m = b(t_s\rho_s + t_p\rho_p), \tag{9}$$

$$z_c = \frac{E_s\frac{t_s^2}{2} - E_p\frac{t_p^2}{2}}{t_p + t_s}, \tag{10}$$

$$\alpha = bd_{31}/S_{E_{11}}, \tag{11}$$

$$C_p' = (b/t_p)\epsilon_{33}^T - d_{31}^2/S_{E_{11}}. \tag{12}$$

The coupled system of equations can be written in matrix form, equation (13), where $\mathbf{A_i}$ and $\mathbf{B_i}$ are the coefficient matrices for the two subregions of the unit cell.

$$\mathbf{A_i}\frac{\mathrm{d}\mathbf{z}(x)}{\mathrm{d}x} = \mathbf{B_i}\mathbf{z}(x), \tag{13}$$

$$\mathbf{z}(x) = \begin{bmatrix} w \\ w_x \\ Q \\ M_b \\ V \\ I \end{bmatrix} \quad \mathbf{A_1} = \begin{bmatrix} 1 & 0 & 0 & 0 & 0 & 0 \\ 0 & EI & 0 & 0 & 0 & 0 \\ 0 & 0 & 1 & 0 & 0 & 0 \\ 0 & 0 & 0 & 1 & 0 & 0 \\ 0 & 0 & 0 & 0 & 1 & 0 \\ 0 & 0 & 0 & 0 & 0 & 1 \end{bmatrix}$$

$$\mathbf{z}(x) = \begin{bmatrix} w \\ w_x \\ Q \\ M_b \\ V \\ I \end{bmatrix} \quad \mathbf{A_2} = \begin{bmatrix} 1 & 0 & 0 & 0 & 0 & 0 \\ 0 & EI & 0 & 0 & 0 & 0 \\ 0 & 0 & 1 & 0 & 0 & 0 \\ 0 & 0 & 0 & 1 & 0 & 0 \\ 0 & 0 & 0 & 0 & 1 & 0 \\ 0 & 0 & 0 & 0 & 0 & 1 \end{bmatrix}$$

$$\mathbf{B_1} = \begin{bmatrix} 0 & 1 & 0 & 0 & 0 & 0 \\ 0 & 0 & 0 & 1 & \alpha\left(\frac{t_p}{2} + z_c\right) & 0 \\ -m\omega^2 & 0 & 0 & 0 & 0 & 0 \\ 0 & 0 & -1 & 0 & 0 & 0 \\ 0 & 0 & 0 & 0 & 0 & 0 \\ 0 & \frac{-\mathrm{i}\omega\alpha}{EI}\left(\frac{t_p}{2} + z_c\right) & 0 & 0 & -\mathrm{i}\omega\left(C_p' + \frac{\alpha^2}{EI}\left(\frac{t_p}{2} + z_c\right)^2\right) & 0 \end{bmatrix}$$

$$\mathbf{B_2} = \begin{bmatrix} 0 & 1 & 0 & 0 & 0 & 0 \\ 0 & 0 & 0 & 1 & 0 & 0 \\ -m\omega^2 & 0 & 0 & 0 & 0 & 0 \\ 0 & 0 & -1 & 0 & 0 & 0 \\ 0 & 0 & 0 & 0 & 0 & \frac{\mathrm{i}\omega L + R}{(1-\beta)a} \\ 0 & 0 & 0 & 0 & 0 & 1 \end{bmatrix}$$

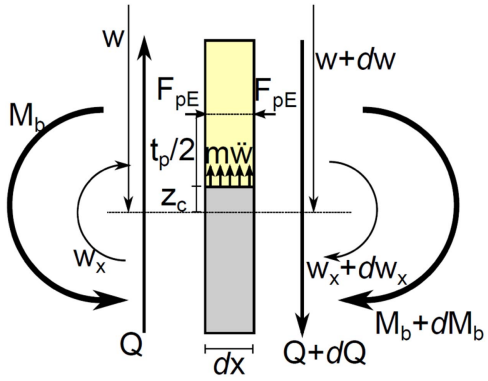

Figure 7. Force and moment equilibria on the infinitesimal element of bilayer beam (substrate and piezoelectric).

4.2. Modeling subregion 2

Even though the second subregion has no electromechanical coupling, energy can travel along the electrical and mechanical waveguides. The electrical waveguide is characterized by the distributed impedance Z', where L and R represent the inductance and resistance, respectively.

$$Z' = \frac{Z}{(1-\beta)a} = \frac{\mathrm{i}\omega L + R}{(1-\beta)a}. \tag{14}$$

The current flowing into the infinitesimal element is the same as the current flowing out, leading to a null spatial derivative of the current.

$$\frac{\mathrm{d}I}{\mathrm{d}x} = 0. \tag{15}$$

Conversely, the distributed impedance will influence the spatial derivative of the voltage.

$$\frac{\mathrm{d}V}{\mathrm{d}x} = -Z'I = \frac{\mathrm{i}\omega L + R}{(1-\beta)a} I. \tag{16}$$

The system of equations describing the mechanical behavior of the second subregion, equations (17)–(20), can be deduced from the ones of the first subregion by setting the piezoelectric element thickness to zero, $t_p = 0$.

$$\frac{\mathrm{d}w}{\mathrm{d}x} = w_x, \tag{17}$$

$$EI\frac{\mathrm{d}w_x}{\mathrm{d}x} = EIw_{xx} = M_b, \tag{18}$$

$$\frac{\mathrm{d}Q}{\mathrm{d}x} = m\ddot{w}, \tag{19}$$

$$\frac{\mathrm{d}M_b}{\mathrm{d}x} = -Q. \tag{20}$$

Without the piezoelectric element, the bending stiffness and mass simplify to equations (21) and (22).

$$EI = E_s I_s = E_s b\frac{t_s^3}{12}, \tag{21}$$

$$m = bt_s\rho_s, \tag{22}$$

By inverting $\mathbf{A_1}$ and $\mathbf{A_2}$ the final form of the system is given by equation (23).

$$\mathbf{C_1} = \mathbf{A_1^{-1}B_1} \qquad \mathbf{C_2} = \mathbf{A_2^{-1}B_2}. \tag{23}$$

Using the matrix exponential, equation (24) is obtained

$$\mathbf{T_1} = e^{a(\beta)\mathbf{C_1}} \qquad \mathbf{T_2} = e^{a(1-\beta)\mathbf{C_2}}. \tag{24}$$

The unit cell transfer matrix is then defined by equation (25).

$$\mathbf{T} = \mathbf{T_2T_1}. \tag{25}$$

The transfer matrix describes the relation between the status vector $\mathbf{z}(x)$ at the beginning, and at the end of the cell $\mathbf{z}(x+a)$.

$$\mathbf{z}(x+a) = \mathbf{T}\mathbf{z}(x). \tag{26}$$

The Bloch–Floquet theorem is used to compute the frequency dependent wavenumber, k. This theorem relates $\mathbf{z}(x+a)$ and $\mathbf{z}(x)$ through a periodic boundary condition which depends on the wavenumber.

$$\mathbf{z}(x+a) = \mathbf{z}(x)\mathrm{e}^{-\mathrm{i}ak}, \tag{27}$$

$$\mathbf{T}(\omega)\mathbf{z}(x) = \mathbf{z}(x)\mathrm{e}^{-\mathrm{i}ak}. \tag{28}$$

Analogously, we can relate both ends to the unit cell using the transfer matrix method, equation (26).

$$(\mathbf{T}(\omega) - \mathrm{e}^{-\mathrm{i}ak}\mathbf{I})\mathbf{z}(x) = 0. \tag{29}$$

Combining equations (26) and (29) yields a standard eigenvalue problem, equation (30). From the solution to the eigenvalue problem, equation (31) is obtained yielding the frequency dependent wavenumber. The real part of the wavenumber portrays information on the propagation of the wave while the imaginary part describes the attenuation. From equation (31) the dispersion curves for the hPC are plotted over the chosen frequency range.

$$\mathbf{T}(\omega) - \lambda\mathbf{I} = 0 \quad \text{with} \quad \lambda(k) = \mathrm{e}^{-\mathrm{i}ak}, \tag{30}$$

$$k(\omega) = \frac{\ln(\lambda)}{-\mathrm{i}a}. \tag{31}$$

5. Experimental setup

The PFVI was designed with a conductive metal pad to interface with the electrode of the piezoelectric element to form an electromechanical entity. Since, this first array of interconnected PFVI was intended as a test bench it was printed on a standard rigid FR4 PCB substrate. Although, the printed array of PFVI only had a thickness of 0.9 mm, it was still sufficiently rigid to act as an additional mechanical waveguide if directly interfaced with the piezoelectric elements. Hence, the array of interconnected PFVI was connected to each piezoelectric element with electrical wires as seen in figure 8.

We excited the structure using an additional piezoelectric element attached approximately in the same position where the discrete force was applied in the numerical model. The piezoelectric element was excited with a sine sweep spanning from 100 to 20 kHz, and an applied voltage amplitude of 10 VPP using a high voltage power amplifier. The out-of-plane velocity

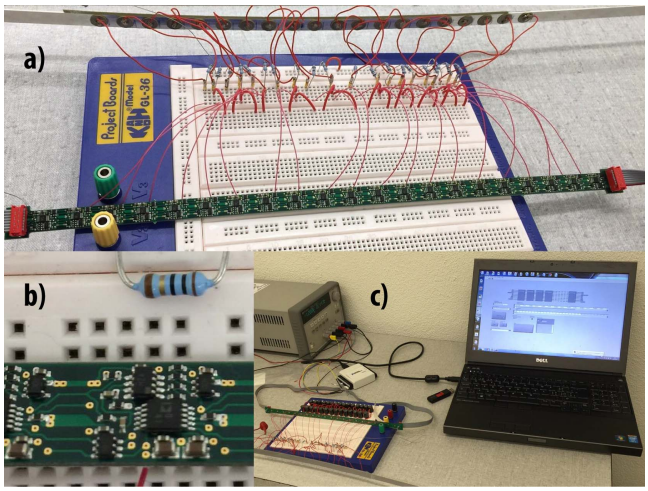

Figure 8. (a) Experimental array of PFVI connected to finite sample of 1D hPC. (b) Close up of one PFVI, compared to a solid resistor. (c) Experimental setup of 1D hPC, and computer for programming array of PFVI.

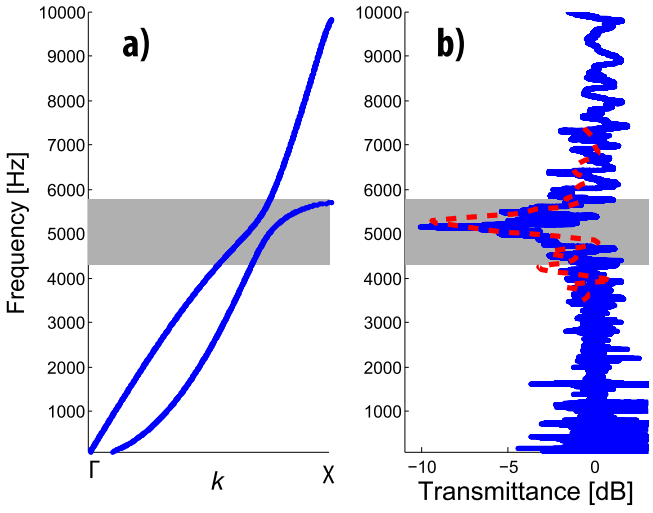

Figure 9. (a) Dispersion monoatomic unit cell $L = 1$ H, with eigenvalue veering between the transverse mechanical and electrical modes. (b) Experimental transmittance (solid line), and numerical transmittance (dotted line) for finite hPC with monoatomic configuration $L = 1$ H.

on the surface of sample was measured using a Polytec PSV 400 scanning laser vibrometer. The transmission properties of the hPC were calculated based on velocity amplitude averaged over regions extending 100 mm on either side of the hPC. We carried out a Fast Fourier transform of the time-domain data for the out of plane velocity along the length of the sample to obtain the frequency response. The numerical investigation was carried out conceptually in the same way, except that the response of the system was investigated directly in the frequency domain.

6. Results and discussion

Figures 9 and 10 show the dispersion and transmittance curves of the monoatomic (single inductance value across all

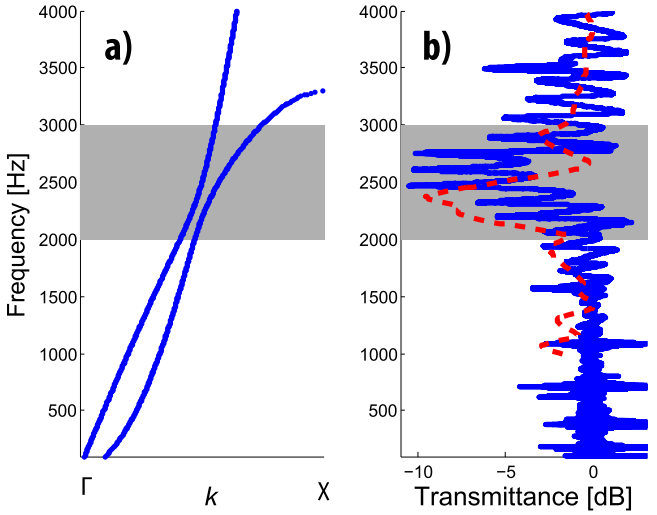

Figure 10. (a) Dispersion monoatomic unit cell $L = 3$ H, with eigenvalue veering between the transverse mechanical and electrical modes. (b) Experimental transmittance (solid line), and numerical transmittance (dotted line) for finite hPC with monoatomic configuration $L = 3$ H.

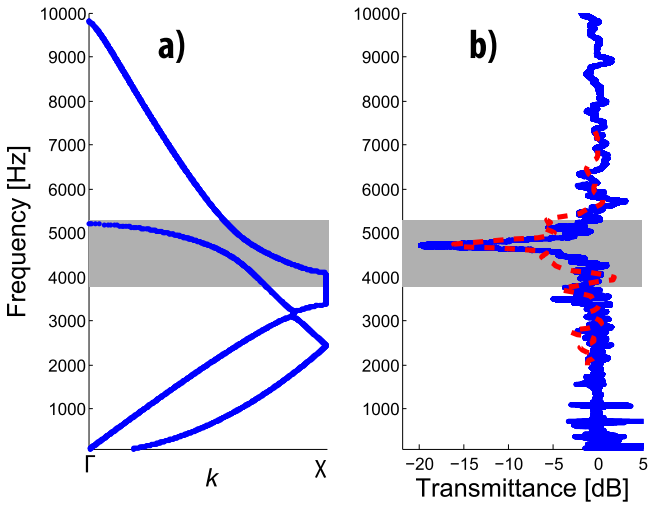

Figure 11. (a) Dispersion diatomic unit cell $L_1 = 1$ H and $L_2 = 1.5$ H, with eigenvalue veering between the transverse mechanical and electrical modes. (b) Experimental transmittance (solid line), and numerical transmittance (dotted line) for finite hPC with diatomic configuration $L_1 = 1$ H and $L_2 = 1.5$ H.

cells) unit cell configuration, for two different inductance values. In figures 9(a), 10(a) we can see that mode coupling occurs in the form of veering. As expected veering occurs at a lower frequency with increasing inductance value. Moreover, in agreement with the work of Bergamini *et al* [4] figures 9(b) and 10(b) show that the regions of low transmittance are centered around the frequency of the mode veering. Moreover, the experimental transmittance curves (solid blue) are in good agreement with the numerical transmittance results obtained from COMSOL (solid red line) in both the frequency range of attenuation as well as the amplitude.

To further exploit the control of elastic waves utilizing the potential to program the individual inductances of the

hPC, a diatomic unit cell configuration with alternating inductance values $L_1 = 1$ H and $L_2 = 1.5$ H was investigated and shown in figure 11. Just as for the monoatomic configuration, the analytical dispersion curves show the presence of mode veering over the same frequency range corresponding to low transmittance in the numerical and experimental curves.

These results indicate that varying the parameters of the electrical domain has a paramount effect on the mechanical properties of the hPC. Furthermore, the potential to instantaneously and accurately retune the electrical parameters, thus reconfigure the hPC, gives way to a versatile lightweight 'smart' material for wave attenuation.

7. Conclusion

In this work, we have demonstrated a high level of integration between the electrical and mechanical domains of a hPC unit cell to create an artificial 'smart' material. Useful and unusual material properties are achieved by focusing 'material development' efforts on the design and implementation of a suitable analog circuit. This approach may represent a new paradigm in the development of materials with novel programmable properties similar to the introduction of electronic components into a number of devices and machines that in the last century were traditionally 'purely mechanical', such as car engines, and typewriters. The inclusion of a digital interface (digital potentiometer) in an otherwise analog circuit, opens the doors to the integration of centralized or, probably more advantageous distributed computing power. Building blocks for the implementation of such distributed intelligence are presented, for example in the work by Shen *et al* [25]. This intimate integration of mechanical components with analog and digital electronic counterparts will allow for the closed loop control of the mechanical properties of the hybrid material in a first stage.

Further work is under way to fabricate the electrical domain of the hPC on a flexible or even stretchable substrate, such as the ones presented by Salowitz *et al* [26], for a higher and seemless level of integration. Alternatively, the mechanical domain could serve as the substrate for the circuitry of the electrical waveguides and associated digital components. Beyond the demonstration of facile tunability of the mechanical dispersion properties of a hPC, that offers a glimpse into the opportunities offered by the hybridization of mechanical and electrical waveguides, we believe that the contribution of the present paper is a first paramount step towards a true integration of electrical and mechanical design of advanced materials.

Acknowledgment

This research was funded by the Swiss National Science Foundation (SNSF, Grant No. 200021 157060), and the Mexican National Science Foundation (CONACYT).

References

[1] Hollkamp J J 1994 Multimodal passive vibration suppression with piezoelectric materials and resonant shunts *J. Intell. Mater. Syst. Struct.* **5** 49–57
[2] Beck B S, Cunefare K A, Ruzzene M and Collet M 2011 Experimental analysis of a cantilever beam with a shunted piezoelectric periodic array *J. Intell. Mater. Syst. Struct.* **22** 1177–87
[3] Spadoni A, Ruzzene M and Cunefare K 2009 Vibration and wave propagation control of plates with periodic arrays of shunted piezoelectric patches *J. Intell. Mater. Syst. Struct.* **20** 979–90
[4] Bergamini A E, Zündel M, Parra E A F, Delpero T, Ruzzene M and Ermanni P 2015 Hybrid dispersive media with controllable wave propagation: a new take on smart materials *J. Appl. Phys.* **118** 154310
[5] Lossouarn B, Deü J and Aucejo M 2015 Multimodal vibration damping of a beam with a periodic array of piezoelectric patches connected to a passive electrical network *Smart Mater. Struct.* **24** 115037
[6] Dell'Isola F, Maurini C and Porfiri M 2004 Passive damping of beam vibrations through distributed electric networks and piezoelectric transducers: prototype design and experimental validation *Smart Mater. Struct.* **13** 299
[7] Batra R C, Dell'Isola F, Vidoli S and Vigilante D 2005 Multimode vibration suppression with passive two-terminal distributed network incorporating piezoceramic transducers *Int. J. Solids Struct.* **42** 3115–32
[8] Maurini C, Dell'Isola F and Vescovo D Del 2004 Comparison of piezoelectronic networks acting as distributed vibration absorbers *Mech. Syst. Signal Process.* **18** 1243–71
[9] Alessandroni S, Andreaus U, Dell'Isola F and Porfiri M 2004 Piezo-electromechanical (pem) kirchhoff-love plates *Eur. J. Mech.* A **23** 689–702
[10] Fleming A J and Moheimani S R 2003 Adaptive piezoelectric shunt damping *Smart Mater. Struct.* **12** 36
[11] Brillouin L 1946 *Wave Propagation in Periodic Structures: Electric Filters and Crystal Lattices* (New York: McGraw-Hill)
[12] Deymier P A 2013 *Acoustic Metamaterials and Phononic Crystals* vol 173 Springer Science & Business Media) (Heidelberg: Springer)
[13] Krödel S, Delpero T, Bergamini A, Ermanni P and Kochmann D M 2014 3d auxetic microlattices with independently controllable acoustic band gaps and quasi-static elastic moduli *Adv. Eng. Mater.* **16** 357–63
[14] Liu Z, Zhang X, Mao Y, Zhu Y, Yang Z, Chan C and Sheng P 2000 Locally resonant sonic materials *Science* **289** 1734–6
[15] Wu T-T, Huang Z-G, Tsai T-C and Wu T-C 2008 Evidence of complete band gap and resonances in a plate with periodic stubbed surface *Appl. Phys. Lett.* **93** 111902
[16] Lee J-H, Singer J P and Thomas E L 2012 Micro-nanostructured mechanical metamaterials *Adv. Mater.* **24** 4782–810
[17] Robillard J-F, Matar O B, Vasseur J, Deymier P A, Stippinger M, Hladky-Hennion A-C, Pennec Y and Djafari-Rouhani B 2009 Tunable magnetoelastic phononic crystals *Appl. Phys. Lett.* **95** 124104
[18] Airoldi L and Ruzzene M 2011 Wave propagation control in beams through periodic multi-branch shunts *J. Intell. Mater. Syst. Struct.* **22** 1567–79
[19] Casadei F, Delpero T, Bergamini A, Ermanni P and Ruzzene M 2012 Piezoelectric resonator arrays for tunable acoustic waveguides and metamaterials *J. Appl. Phys.* **112** 064902

[20] Collet M, Cunefare K A and Ichchou M N 2009 Wave motion optimization in periodically distributed shunted piezocomposite beam structures *J. Intell. Mater. Syst. Struct.* **20** 787–808
[21] Bergamini A, Delpero T, Simoni L D, Lillo L D, Ruzzene M and Ermanni P 2014 Phononic crystal with adaptive connectivity *Adv. Mater.* **26** 1343–7
[22] Mace B R and Manconi E 2012 Wave motion and dispersion phenomena: Veering, locking and strong coupling effects *J. Acoust. Soc. Am.* **131** 1015–28
[23] Airoldi L, Senesi M and Ruzzene M 2012 Piezoelectric superlattices and shunted periodic arrays as tunable periodic structures and metamaterials *Wave Propagation in Linear and Nonlinear Periodic Media* (Berlin: Springer) pp 33–108
[24] von Grunigen D C, Ramseier D and Moschytz G 1986 Simulation of floating impedances for low-frequency active filter design *Proc. IEEE* **74** 366–8
[25] Shang Y, Shen Z and Xiao S 2013 On the design of single-layer circuit analog absorber using double-square-loop array *IEEE Trans. Antennas Propag.* **61** 6022–9
[26] Salowitz N P, Guo Z, Kim S-J, Li Y-H, Lanzara G and Chang F-K 2014 Microfabricated expandable sensor networks for intelligent sensing materials *IEEE Sens. J.* **14** 2138–44